Towards a Discrete Snake-like Robot Based on SMA-actuated Tristable Modules For Follow The Leader Control Strategy

Benjamin Calme, Lennart Rubbert, Yassine Haddab

Towards a Discrete Snake-like Robot Based on SMA-actuated Tristable Modules For Follow The Leader Control Strategy

Benjamin Calmé[1,2], Lennart Rubbert[2] and Yassine Haddab[1]

***Abstract*—Snake-like robots applications include surveillance and exploration of confined environments where human presence is incompatible. The attractiveness of this type of mechatronic structure is notably linked to the modular character and the hyper-redundancy of their architecture, which gives it both mechanical robustness and great manoeuvrability. However, due to the large number of degrees-of-freedom, the use of advanced mathematical models are needed to asses the motion patterns and to simulate it. A new snake-like robot architecture is introduced in this paper together with the development methodology of a replicable multistable module. The interest of this contribution lies in the combination of the mechanical stability of the modules with an easy-to-use direct kinematic model, thus avoiding the need of complex control strategies.**
The design of one module exploiting the three stable states of a tristable flexible mechanism so as to orient the articulation of the module at three distinct stable angles is first presented. Then a prototype of a modular snake-like robot is built and experimentally evaluated. The prototype consists of 4 modules that can be individually oriented by $\pm$7.1 degrees. Each module measures 51.5x32mm and weighs 2.5g. Thereby, this work provides the first results on the feasibility of this robotic architecture which consists of several multistable modules. A good agreement between the working space estimated with the direct kinematic model and experimental measurements is obtained. According to the fact that these are preliminary results, there is a 1.5% error between the experimental results and the models.

***Index Terms*—Compliant Joints and Mechanisms; Mechanism Design; Redundant Robots**

I. Introduction

FIRST snake-like robots can be found in the early 1970s [1]. These robots are used in several fields due to their ability to move in constrained spaces according to complex trajectories. They can be found in the maintenance of dangerous structures such as pipelines and nuclear plants [2]. They also have potential applications in space as robotic manipulators due to their high dexterity. In addition, their robustness, linked to their large kinematic redundancy, allows to maintain performance in the case of partial damage [3]. More recently, they have also found interest in the medical field, in the context of Natural Orifice Transluminal Endoscopic Surgery (NOTES), as they can adapt to various anatomies, but also thanks to their ability to follow the movement of organs during the surgical procedure, i.e. breathing [4]. Due to their use in particularly demanding areas, these robots must meet operating constraints inherent to these applications. This becomes especially true when dealing with miniaturisation issues. Snake-like robots are often bulky on a macroscopic scale. The transition to the mesoscopic scale is generally made by scaling down the traditional components used in anthropomorphic or in cable robots. However, the miniaturisation of motors and their complex assembly are challenging. Cable drive, although having the particular advantages of allowing remote actuation and having a small footprint, has limitations related to the friction of the cables within the sheath, yielding control issues due to hysteresis, backlash and overvoltage. This may result in inaccurate positioning and motions of the end-effector [5], [6]. Moreover, snake-like robot designs based on individualised sections with independent actuation have limitations in increasing the number of actuation cables and consequently the friction [7]. Besides, the closed-loop control of snake-like robots with these two types of actuation requires small and expensive sensors. The incorporation of these sensors into a mesoscopic robotic structure is also not trivial. Research on hyper-redundant manipulator with binary actuators has addressed open-loop control alternatives, e.g. the Variable Geometry Truss (VGT) [8], [9], [10]. However, it requires the development of complex kinematic models. In contrast, an architecture exploiting the mechanical properties of bistable mechanisms [11] has simplified control laws, e.g. the Dimibot [12] or the BRAID [13]. However, this digital micropositioner has a compactness limitation. The contributions of this paper is to propose :

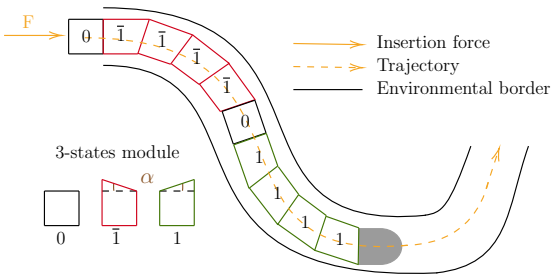

Fig. 1. Principle of the 3-states module based snake-like robot developed to perform complex trajectories in confined environment. Each state of the module is identified as a balanced ternary signed-digit, i.e. $\bar{1}, 0, 1$.

Manuscript received: September, 21, 2022; Accepted November 18, 2022 .
This paper was recommended for publication by Editor C. Gosselin upon evaluation of the Associate Editor and Reviewers' comments. This work was supported by the Investissements d'Avenir (Labex CAMI ANR-11-LABX-0004).

[1]Benjamin Calmé and Yassine Haddab are with LIRMM, Univ Montpellier, CNRS, Montpellier, France. benjamin.calme@lirmm.fr
[2]Benjamin Calmé and Lennart Rubbert are with ICube, University of Strasbourg, France.

Digital Object Identifier (DOI): see top of this page.

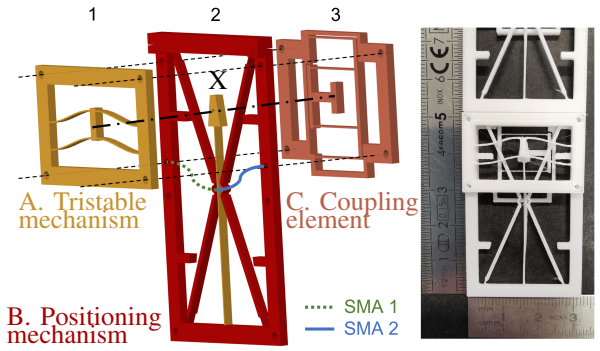

Fig. 2. Tristable module CAD model: Exploded view of the three pieces. The numbers indicate the pieces and the colours and the letters indicate the mechanisms. Actuators are shown schematically for ease of understanding (Left). 3D printed tristable module assembled (Right).

- A multistable module, with three stable states, which must be replicable and can be assembled serially, as illustrated in Fig. 1,
- A new snake-like robot architecture with discrete workspace and simplified open loop control.

The module is designed using compliant mechanisms, which exploit the mechanical properties of materials and which are easily miniaturised [14], [15]. The actuation is carried out with an active material of small size, i.e. Shape Memory Alloys (SMA), and providing the required triggering force [16], [17], [18].

The goal of this paper is to present a new approach to design snake-like robots with a proof of concept. Although no particular application is targeted, it seems that medical applications such as NOTES might be relevant.

The paper is organized as follows. In Section II, the design concepts and the corresponding contributions are introduced. In Section III, the module analytical characterisation is detailed. The forward kinematic model is presented in Section IV. In Section V, the mechanism characterisation and the actuator sizing are described. Then the results of the evaluation of our prototype are discussed in Section VI and the conclusions are given in Section VII.

II. DESIGN CONCEPTS

A. A scalable tristable module

Although the amplitude of elastic deformation is limited and material-dependent, compliant mechanisms have many advantages. They benefit from improved precision and reliability, and from the absence of friction, wear and backlash due to lack of contacts. A bistable mechanism is based on the exploitation of a controlled deformation of the structure following a change in boundary conditions. The most common case in the literature is the well-known double precurved beam bistable mechanism. This type of mechanism lends itself well to miniaturisation through 3D manufacturing or electrical discharge machining [12]. Multistable mechanisms can correspond to an arrangement of bistable mechanisms. Despite the fact that the "T-shape" multistable mechanism is already existing [14], [15], its implementation within a flexible structure in order to design a replicable module has not been presented before. Moreover, to the best of the authors' knowledge, this kind of serial modular robotic architecture based on multistable mechanism has never been studied in literature.

The module is shown in Fig. 2. It consists of three pieces identified by numbers and three mechanisms identified by colours and letters. The module is manufactured in three pieces, as shown in the exploded view.

- The tristable mechanism (A) allows the module configurations to be changed or maintained.
- The flexible positioning mechanism (B) is capable of converting each stable state of A into an angle α in the plane.
- The flexible coupling element (C) is used to ensure the maintenance of the boundary conditions for the proper functioning of A and B.

As show in Fig. 2, note that A belongs to both pieces 1 and 2. This answers a design constraint detailed in Subsection III-A. The coupling element will only be briefly detailed in this article. The combination of these three mechanisms forms a module as shown in Fig. 2 (Right).

B. Distributed actuation snake-like robot

An ideal snake-like robot only requires energy input when changing configuration. However, in practice, whether it is a motor drive or a cable drive, energy is consumed to maintain a configuration. This is a feature of multistable mechanisms, whose discrete actuation is linked to a on-off energy input required for triggering. Bistable mechanisms have the advantage that once a stable configuration is reached, it is maintained as long as no energy input generates a deformation towards another stable state. The proposed tristable module also has the advantage of having a low actuating force while being able to withstand large external forces. This type of approach can be interesting in the case of medical robotics where the robot has to maintain a configuration during the time of the procedure, which is difficult to do and energy consuming with the current cable driven robots [5].

The design of the mechanism required the actuator to provide a displacement of a few millimetres and a force of a few Newtons, given the limited space. Of the smart actuators that could be used, only SMAs were able to meet these requirements in terms of deformation and energy density at the same time [19]. Moreover, the design and control of an active endoscope operated by antagonistic SMAs has already been proven [20]. SMA wire deformation is due to a change in the structure of the crystalline phase of the material resulting in a length shortening. This shortening is the consequence of an increase in temperature of the material and the joule effect is usually chosen as the method of actuation. The recovery of the initial length is achieved by the application of mechanical stresses due to the actuation of the oppositely mounted wire, as shown in Fig. 2. The advantage of using small actuators and short current pulse actuation is that it requires only minimal heat generation, thus requiring little dissipation.

C. Simplified open-loop control

The literature includes studies of open-loop controllable manipulators, such as the VGT manipulator [8], which provides performance in hyper redundant 2-D space using binary actuators. Due to its high redundancy and kinematic architecture, complex direct and inverse kinematic models had to be developed. The digital microrobot, Dimibot [12], offers some answers to these problems. Thanks to its architecture based on bistable mechanisms, this discrete robot simplifies the control laws. This is also true with the use of multistable mechanisms that allows the precise configuration of a module to be known. As each module is serially assembled and independently controlled, global configuration of a multi-modular snake-like robot can easily be known. Thereby, it allows to consider control strategies such as *follow-the-leader* approach. This progression strategy, which is particularly desirable for applications in constrained environments or exploiting tortuous trajectories, is characterised by the fact that the hyper-redundant or continuum robot body follows the path traced by the head [21], [22], i.e. the distal module.

III. Analytical Modelling of Mechanisms

A. Tristable mechanism design

The tristable mechanism is based on a combination of straight and preformed beams rigidly joined together, as shown in Fig. 3. An actuation resulting in a deformation of the straight beam allows the preformed bistable beams to buckle due to the occurrence of a shuttle loading. In the case where SMA 1 is activated, the second stable configuration is reached. Then, the actuation of the SMA 2 will allow a return to the first configuration and then reach the third stable configuration. The holding capability of this buckled configuration is made possible by the difference between the force required to buckle the vertical beam and the force required to actuate the bistable beams. The analytical model is inspired by the work of Hussein et al. [23] and the theory of buckling, in particular the determination of the Euler critical load.

The tristable mechanism is shown in orange in Fig. 2 and in Fig. 3. The model developed in the following sections will represent it as a single unit. However, it was designed with two pieces, namely piece 1 and a part of piece 2 of the mechanism, linked at point X in Fig. 2. This solution was chosen in response to footprint constraints and in order to maximise the buckling of the beam of piece 2.

1) Modelling of the preformed beams of the tristable mechanism

The first part described is the bistable mechanism composed of two superimposed curved beams in a stable state which therefore contains neither deformation energy nor residual stress. This configuration is maintained as long as no force greater than the holding force is applied in the perpendicular direction, along the $\vec{y}$ axis on Fig. 4a. The geometrical parameters of curved beams are: length l, thickness t, width w and initial height h [23]. These quantities are represented in Fig. 4 and whose nominal values were given in Tab. I. The

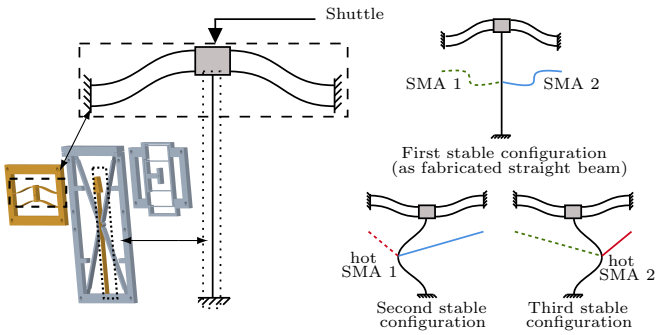

Fig. 3. Representation of a tristable double-beam based mechanism illustrated in its three stable equilibrium positions which will be converted by the positioning mechanism to produce the 3 distinct orientation of the module. The fabricated configuration corresponds to the first stable state. The mechanical correspondence is in orange in the CAD model.

shape of the as-fabricated beams, ω in its initial configuration is described by the following equation:

$$\omega(x) = \frac{h}{2}\left(1 - \cos\left(2\pi\frac{x}{l}\right)\right) \tag{1}$$

The shuttle shown in Fig. 3 and Fig. 4a is inserted at the mid-section of the precurved beams to prevent this section to rotate. However, in order to ensure bistability, according to [24], the following condition on the ratio Q of the apex h to the thickness of the beam t is required :

$$Q = h/t > 2.31 \tag{2}$$

The characteristic curve of the applied force f, along $\vec{y}$ at P, as a function of the displacement of the shuttle center d exhibits two extrema values, identified in Fig. 4a, which are obtained using the following equations [24]:

$$f_{top}, f_{bot} = \frac{Ewt^3h}{l^3}\frac{32\pi^2}{9}\left(\frac{4}{9} \mp \pi\sqrt{\frac{1}{6} + \frac{16}{81\pi^2} - \frac{1}{Q^2}}\right) \tag{3}$$

$$d_{top}, d_{bot} = h\left(\frac{28}{27} \pm \frac{2\pi}{3}\sqrt{\frac{1}{6} + \frac{16}{81\pi^2} - \frac{1}{Q^2}}\right) \tag{4}$$

The values obtained from the previous equations make it possible to identify the maximum force values, i.e f_{top} and f_{bot}, to be provided in order to operate the mechanism and the stroke value for which the following are obtained, i.e d_{top} and d_{bot}. Due to the manufactured initial precurved shape, the value of the snapping force is not symmetric for leaving the stable configurations. The force f_{top}, which is greater than f_{bot} is the maximal reaction force of the bistable mechanism, as shown in Fig. 4a and later in the results Fig. 8, therefore the actuator must be able to provide a force greater than f_{top}.

2) Modelling of the vertical beam of the mechanism

The second part of the mechanism, represented in Fig. 4b, concerns the initially vertical beam whose buckling initiated by the actuators will result in large deflections and a sudden change of configuration of the bistable mechanism. The choice of using an initially straight beam is justified here by obtaining a symmetrical snap-through behaviour between the two buckling sides. This beam therefore has an initial stable configuration and two buckled stable configurations.

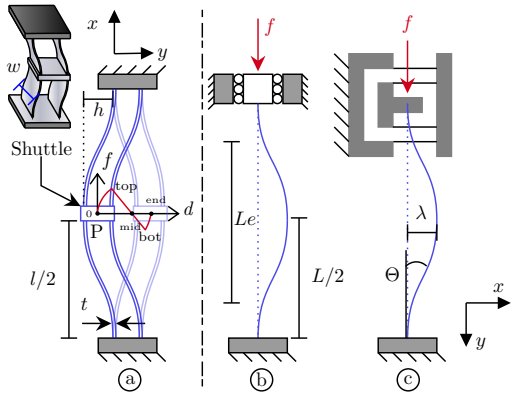

Fig. 4. Representation of a precurved bistable mechanism and the evolution of the force f as a function of the position d (subfigure a). The subfigures b and c illustrate respectively a buckling beam with a theoretical guided-fixed end condition and in the real end condition with a slider.

TABLE I
TRISTABLE MECHANISM DESIGN PARAMETERS

	Parameters	Mechanism
Bistable mechanism	E	1944MPa
	t	0.25mm
	h	2mm
	l	23mm
	w	1.5mm
Vertical beam	ζ	0.7
	L	34mm
	t	0.4mm
	w	1.5mm
	σ_{adm}	55MPa

In order for the beam to buckle, the following condition must be met [25]:

$$f \geq \frac{\pi^2 EI}{(\zeta L)^2}. \tag{5}$$

This equation describes the minimum force that can trigger the buckling of a beam whose material and geometrical parameters are known. These parameters are the Young modulus of the material E, the second moment of area I, the actual length L and the effective length factor ζ, i.e. a ratio to obtain the effective length L_e as a function of the length of the beam, as illustrated in Fig. 4. L_e corresponds to the section of the beam between two inflection points (zero bending moment points) on the buckled shape for a specific type of connection, a pined-fixed beam in this case according to experimental results. This minimum force must be lower than the force f_{bot} described above for the bistable mechanism. Considering the slenderness ratio, $t << l$, and the vertical beam boundary conditions, the maximal stress, σ_{max}, is estimated using Euler's formula [25]

$$\sigma_{max} = \frac{\pi^2 E}{(\zeta L/r)^2} \quad \text{with} \quad \sigma_{max} \leq \sigma_{adm} \tag{6}$$

where r is the radius of gyration of the cross section. The σ_{max} value was calculated and compared to an admissible stress value σ_{adm}, defined according to the yield strength of the material, in order to ensure the proper functioning of the mechanism.

The boundary conditions are controlled by means of a flexible slider inspired by that used by Rubbert et al. [26] and represented in Fig. 4c.

The two elements described above form the first mechanism that provides the three stable configurations of the module. It will be associated with the mechanism described in the following section which will provide angle orientation.

B. Positioning compliant mechanism

1) Mechanism descriptions

The positioning mechanism can be modelled as a 6-bar mechanism as shown in Fig. 5. The symmetry of this mechanism makes it possible to simplify the geometrical model and to analyse only half of it. Links named by letters in the geometric model are shown on the CAD model to illustrate their correspondence.

This mechanism must deform under the effect of the tristable mechanism and produce an angle α. This angle is both the one of the mechanism and the one of the module. In addition, this mechanism must ensure that these orientations are maintained. This is ensured by mechanical stoppers. The module configurations must be maintained against forces external to the module, i.e. the weight of successive modules and, in the future, the forces that may result from contact with the environment.

2) Sustainable forces

Although this mechanism is subsequently linked to the tristable mechanism previously described, these two mechanisms are partially decoupled to isolate the multistable mechanism from external solicitations when it is not actuated.

As the structure of this mechanism is composed of flexible hinges, over-constraints due to external interactions must be taken into account during the design. These constraints are included by means of a safety coefficient and mechanical stoppers. Those stoppers have a double purpose, they prevent deformations beyond the elastic limit and allow the transmission of the forces acting on the mechanism. The flexible linkages used for this prototype, as shown in Fig. 5, are modelled as thin section beams. Cross spring hinges are normally preferred due to their advantageous kinematic performance and better stress tolerance. However, in the case of this prototype, these hinges were preferred due to their smaller footprint and manufacturing constraints. As the resolution of the printer limits the printing of notched hinges, this type of hinge was therefore designed and modelled as a beam, whose loading could be similar to that of a cantilever beam loaded at the ends. This model was carried out in accordance with beam theory [27] such as $\beta = (Fl_{hinge}^2)/(2EI)$ and $\sigma_{max_h} = My/I$, where β is the slope, F is the force exerted by the tristable mechanism, l_{hinge} is the length of the joint, and M and y are the moment and distance to the neutral axis. The maximal constraint σ_{max_h} was compared to the same admissible stress criteria as previously defined σ_{adm}. The mechanical stoppers have been sized so as not to exceed the allowable stroke, $\beta = 14°$, and constraint, $\sigma_{max_h} = 53.33MPa$, values of these hinges.

For practical reasons, it was chosen to size a prototype to 8 modules in this article. This implies that, in the worst

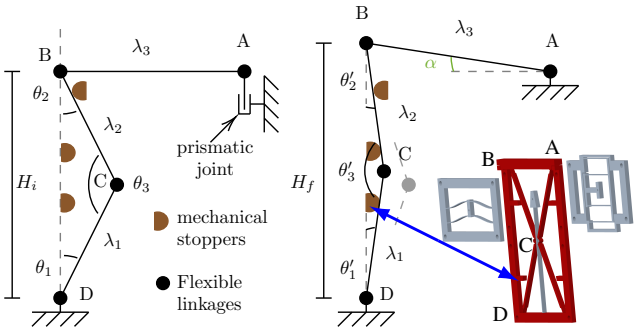

Fig. 5. Geometric model of half of the compliant structure in initial configuration on the left and deflected on the right. Mechanical correspondence in the initial configuration in red in the CAD model.

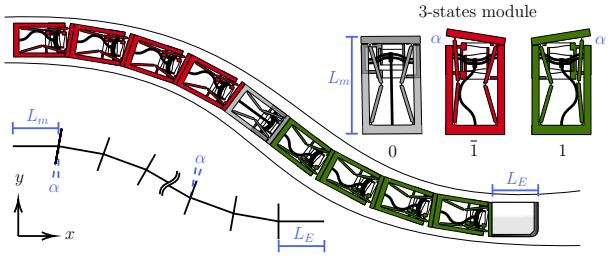

Fig. 6. Representation of a tristable double-beam based mechanism illustrated in its three stable equilibrium positions and their integration into the module based snake-like robot. The fabricated configuration corresponds to the first stable state.

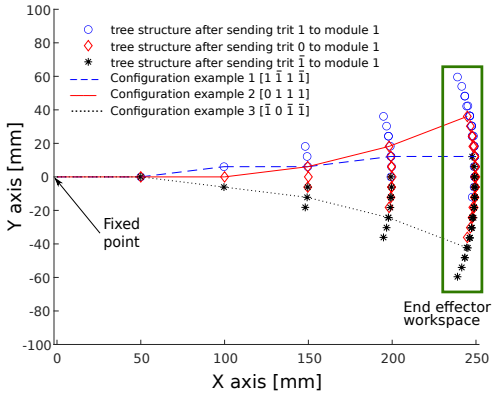

Fig. 7. End-effector workspace generated for a 4-module architecture with fixed proximal end and some configuration examples.

case, the most proximal module must support and be able to be actuated against the weight of the other seven modules. It was therefore necessary to take into account the weight of each module, which is 2.5g, and the weight of future printed circuit boards (PCB), also estimated at 2.5g. The weight of a module was not a design criterion for this prototype and was measured afterwards. Knowing the length, L_m, and the weight of each i module, W_i, and the number of modules, n, it can be calculated the moment that this module will have to sustain, $\Sigma_{i=1}^{n-1=7} i L_m W_i$, i.e. 5.5N (560g). The dimensioning will be done with a safety coefficient justifying to consider 7N.

3) Mechanism geometrical model

If we refer to the geometrical model of the structure shown in Fig. 5, the objective is to maximise the mechanism orientation given by the signed angle α. For our prototype this angle is set at 7°. This angle value may seem low, but within the flexible mechanisms, it already belongs to the long stroke mechanisms. This value may be subject to further optimisation in order to be increased. Once actuated, due to the constraints on the stoppers, it is possible to neglect the vertical displacement at A and assume that it is fixed.

Then the length λ_k of the segments, represented in Fig. 5, is determined using the following equations, knowing that the θ_k represent the angles between the segments, that H_i represents the initial height of our mechanism and H_f the height once the structure is deformed by the tristable mechanism.

$$\alpha = \arcsin(H_f - H_i) \tag{7}$$

$$H_i = \lambda_1 \cos\theta_1 + \lambda_2 \cos\theta_2 \tag{8}$$

$$H_f = \lambda_1 \cos\theta'_1 + \lambda_2 \cos\theta'_2 \tag{9}$$

IV. Forward Kinematic Model

The module has been designed to produce a signed angle α. An adaptation of Fig. 1 is shown in Fig. 6 taking into account the actual design of the modules and illustrating the achievement of α. In the same figure, the kinematic model of the robot has also been represented using a bar chart. The position of the end effector with respect the robot fixed base can be expressed as a function of the state of every tristable module:

$$\begin{bmatrix}\delta_{Ex}\\ \delta_{Ey}\end{bmatrix} = \begin{bmatrix} L_m + \sum_{i=1}^{n} L_m \cos(\sum_{j=1}^{i}\alpha_j) + L_E \cos(\sum_{j=1}^{i+1}\alpha_j) \\ \sum_{i=1}^{n} L_m \sin(\sum_{j=1}^{i}\alpha_j) + L_E \sin(\sum_{j=1}^{i+1}\alpha_j) \end{bmatrix} \tag{10}$$

where i and $i+1$ are the module number, the end effector number. L_E is the length of the end effector.

This kinematics generates a discrete 2D workspace linked to the specifications established for the design of tristable modules. In the case of a superposition of 4 tristable modules, as it will be the case with the prototype used hereafter, the workspace is composed of 81 partially redundant discrete positions distributed in a Cartesian workspace, Fig. 7 . All these positions can be addressed using a 4-trit ternary word consisting of the state of each tristable module. The trit is a bit analogue belonging to the ternary numerical system, i.e. expressed in a base 3. More specifically, a balanced ternary signed-digit representation is used. This digit set is $\mathcal{D} = (\bar{1}, 0, 1)$.

The size of the workspace can be improved by increasing the number of modules. As mentioned earlier, the number of discrete final positions follows a 3^n law, e.g. by doubling the number of tristable modules, the number of reachable points becomes 6561 (addressable on a 8-trit ternary word).

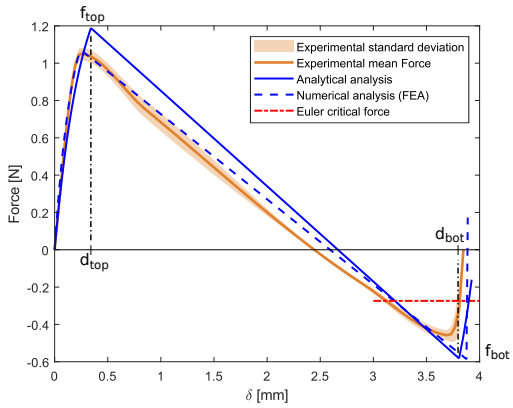

Fig. 8. Force-Displacement curves of the bistable mechanism: analytical model presented in continuous line, Finite Element Analysis (FEA) in dashed line and experimental results conducted on 10 mechanisms in orange.

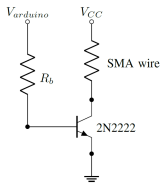

Fig. 9. Electrical circuit for actuating the SMAs.

V. MECHANISM CHARACTERISATION AND ACTUATORS SIZING

A. Tristable mechanism characterisation

In order to characterize the tristable mechanism, the following setup was used. It is composed of a force sensor (FK50, Sauter) able to measure a force up to 50 N with an accuracy of 0.02 N, and a laser-based displacement sensor (LK-H152, Keyence) capable of measuring a displacement in a range of 80 mm with a resolution of 0.25μm.

The force is applied on the shuttle of the bistable mechanism by moving the linear table on which the force sensor is mounted and the induced displacement is measured using the displacement sensor. In order to determine the negative forces, the bistable mechanism has been reversed.

This setup is not illustrated in this article but is identical to the one used in previous experiments [28]. The results from this experiment are presented in Fig. 8 and are compared with the results from the analytical model and finite element analysis performed in Creo Simulate. The measured experimental results are in good accordance with what was estimated analytically and especially numerically.

The force was also applied on the vertical beam until the buckling. The average value measured was 0.28 N allowing to validate the correspondence with the previously calculated critical force Eq. 5 which is consistent with the expected values. The minimum displacement linked to buckling was also estimated at 1.3 mm, in order to size the actuators, i.e. SMA wires.

B. SMA wires actuators sizing

The SMA wires used in the design of the module are from Dynalloy Inc. (CA, United States). The selection of these wires was based on their transition temperature and the dimensioning of the mechanisms carried out beforehand. Regarding the transition temperature of the SMA wires, the choice was made to use 70°C in order to do not risk of damaging the prototype, which for this test was made of polycarbonate and whose supplier describes a conservation of mechanical properties up to 80°C. In addition, considering higher temperature limits the cooling time and gives a higher heating/actuation time ratio.

In order to actuate the structure, it was experimentally considered necessary to provide a bending displacement of at least 1.3 mm orthogonal to the beam attached to the bistable and an estimated force greater than 1.04 N. The manufacturer describes a maximum shortening of approximately 5%, so the wire must be at least 26 mm long to achieve the required shortening. Within a small margin of error, the wire length was set at 30 mm. The diameter of the wire was then chosen according to the required force. After some testing, it was found that 150μm wires supporting up to 600 MPa of continuous stress could provide an average force of 1.06 N. This value being higher than the required one, the latter was retained. In view of the required stroke, an SMA wire is currently sufficient to actuate the tristable structure. In the case of future optimisation and the need for a longer stroke, the SMA wire can be replaced by an SMA spring.

The on-off control of each of the SMAs was done using an Arduino Mega, as shown in the Fig. 9. Each of the SMA wires was supplied with a current of 0.1 mA at a voltage of 3V using a power stage.

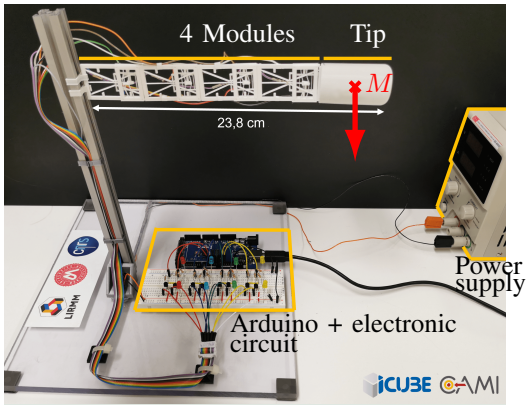

Fig. 10. Prototype with 4 modules in reference position without power supply.

VI. DISCRETE POLYARTICULATED ROBOTIC SYSTEM

Once the feasibility of a module was established, an assembly of 4 modules was made as a proof of concept, visible in Fig. 10. The different modules were held together with glue. The choice of adding a tip with the same weight, M, as the sum of 4 supplementary modules was also made in order to anticipate a future extension.

A. Operating principle and validation protocol

The assembly and operating principle of the robot are shown in Fig. 11. The central wire provides power from the power supply and the side wires are those connecting the SMA wire (〰) to the transistor. To operate the mechanism, the current is apply to the SMA wire of the selected module.

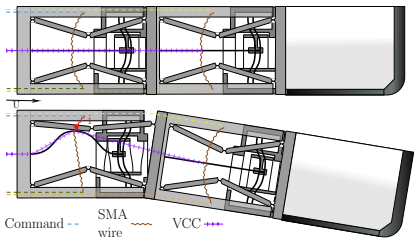

Fig. 11. Schematic representing routing and operating principle.

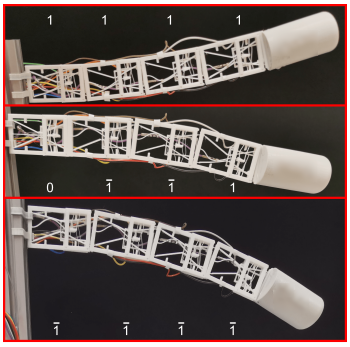

Fig. 12. Photos of three configurations taken by the robot with the associated ternary words.

The wire heats up and shortens inducing the configuration change. Each module being independent, the robot takes a shape defined by a defined sequence. Three of these sequences are shown on Fig. 12. To validate the operation of the robot, a measurement of the position of the tip was carried out for each configuration using graph paper and was compared to the estimated workspace calculated in Matlab.

B. Results and discussion

For each module, before assembly, a measurement of the output angles was made and an average angle of 7.1° was observed. Afterwards, the measurements were carried out and the results are presented in Fig. 13.

Three major points emerged from this first phase of experimentation. The first observation is that the error between the measured position and the estimated position is smaller when the robot is controlled against gravity, a phenomenon already observed in the literature [29]. This result suggests that the torques exerted may result in a greater displacement than was anticipated in the design. It can also be explained by the nature of the material used and the fact that there is still an assembly phase. A study with other materials and monolithic manufacturing will be conducted to investigate these assumptions.

The second remark concerns the redundancy of the work space. For n modules, the robot has 3^n output positions, many of which are redundant and useful for path planning. As describe earlier, each addition of a module significantly increases the number of discrete points in the workspace. The robot has 81 positions as it is, but with the addition of the 4 anticipated extra modules, the workspace will contain 6561 positions. During the measurements, it is observed that, due to some mechanical backlash of the modules, some configurations that should have given the same output position could end

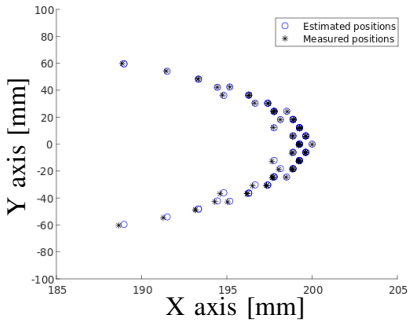

Fig. 13. Representation of the robot's workspace, with the estimated positions in blue ring and the measured positions in black star. A zoom is made along the X-axis with respect to Fig. 6 for the sake of readability.

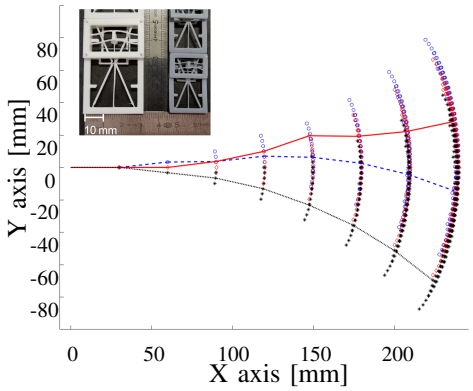

Fig. 14. Photograph of miniaturised modules obtained by stereolithography (in grey) and representation of the achievable workspace, and certain configurations (solid, dashed and dotted lines), with a prototype of equivalent length but composed of the miniaturised module.

up with different values. A repeatability study will be carried out in future work in order to exploit them to enrich the robot's workspace. It is also interesting to note that the workspace as represented corresponds to that of a robot fixed at one end, it is possible to attach it to a linear actuator in a future version. Since the actuations will be performed during a translation the temporal aspect adds interesting perspectives in terms of workspace and control strategy for obstacle avoidance.

The third point concerns the oscillatory aspect of the structure during the actuations. This phenomenon is more important for an actuation performed near the base than at the distal end of the robot and is due to the change of state of the mechanism within the structure. This phenomenon can be limited by control aspects by heating the opposing wire beforehand to use it as a damper or by using friction with the environment.

VII. CONCLUSION

In this paper, a new snake-like robot architecture is presented. The initial focus was on the design of a tristable module that would meet performance criteria, i.e. a long-stroke mechanism requiring low actuation force for high sustainable force, precise positionning and ease of miniaturise and assembly. The mechanical advantages of the tristable modules allows the generation of stable and robust discrete achievable positions, and energy saving due to the sole need for energy input during the switch-over and not to hold positions.

The feasibility of manufacturing by 3D printing has been proven, as well as the principle of actuation by means of

shape memory alloy wires. The results obtained experimentally are consistent with the analytical and numerical models. Accordingly, it was possible to build a n-modules snake-like robot. Once the prototype of the digital robot was assembled, the Cartesian discrete workspace was shown to be in good agreement with the one estimated with a direct kinematic model. Although further research on accuracy and repeatability are still needed, these preliminary results motivate the use in confined spaces such as in medical endoscopy through follow-the-leader and open-loop control.

Further studies dealing with performance optimisation and dynamic oscillation reduction will be performed. Moreover, due to the nature of the mechanisms employed, this prototype faces stiffness issues when subjected to a tensile load. This issue will be addressed through design optimisation and the use of additional stoppers in future versions of the prototype. The first miniaturised modules were obtained by stereolithography, as shown in Fig. 14. This prototype is 33% smaller than the original prototype and allows to obtain an angle of ± 6.3 degrees per module. This size/performance ratio allows to almost follow the Magill curvature, i.e. the angle between the mouth and the throat. After a new miniaturisation phase, still possible with the same process, it could then be considered for example for NOTES applications. Furthermore, 3D printing of composites offers new perspectives for printing actuators and obtaining monolithic structures [30]. It is also envisaged to use other manufacturing processes and materials in order to pursue a more drastic miniaturisation [31]. Then, trajectory planning strategies, which are generally non trivial for discrete workspaces, will be studied using graph theory, i.e. dynamic programming (Bellman) and Hidden Markov model. Three-dimensional displacement can be obtained either by adapting the current design or by alternating the modules by 90 degrees of axial rotation when assembled serially.

REFERENCES

[1] Y. Umetani and S. Hirose, "Biomechanical Study on Serpentine Locomotion Mechanical Analysis and Zoological Experiment for the Stationary Straightforward Movement," *Transactions of the Society of Instrument and Control Engineers*, vol. 8, no. 6, pp. 724–731, 1972.

[2] S. Hirose and A. Morishima, "Design and Control of a Mobile Robot with an Articulated Body," *The International Journal of Robotics Research*, vol. 9, no. 2, pp. 99–114, Apr. 1990.

[3] V. Sujan, M. Lichter, and S. Dubowsky, "Lightweight hyper-redundant binary elements for planetary exploration robots," in *2001 IEEE/ASME International Conference on Advanced Intelligent Mechatronics.*, vol. 2, Jul. 2001, pp. 1273–1278 vol.2.

[4] F. Nageotte, L. Zorn, P. Zanne, and M. De Mathelin, "STRAS: A Modular and Flexible Telemanipulated Robotic Device for Intraluminal Surgery," in *Handbook of Robotic and Image-Guided Surgery*, M. H. Abedin-Nasab, Ed. Elsevier, Jan. 2020, pp. 123–146.

[5] R. A. Porto, F. Nageotte, P. Zanne, and M. d. Mathelin, "Position control of medical cable-driven flexible instruments by combining machine learning and kinematic analysis," in *2019 International Conference on Robotics and Automation (ICRA)*, May 2019.

[6] D. Baek, J.-H. Seo, J. Kim, and D.-S. Kwon, "Hysteresis Compensator with Learning-based Pose Estimation for a Flexible Endoscopic Surgery Robot," in *2019 IEEE/RSJ International Conference on Intelligent Robots and Systems (IROS)*, Nov. 2019, pp. 2983–2989.

[7] Y. Chen, J. Liang, and I. W. Hunter, "Modular continuum robotic endoscope design and path planning," in *2014 IEEE International Conference on Robotics and Automation (ICRA)*, May 2014.

[8] G. Chirikjian, "A binary paradigm for robotic manipulators," in *Proceedings of the 1994 IEEE International Conference on Robotics and Automation*, May 1994, pp. 3063–3069 vol.4.

[9] K. C. Lau, Y. Y. Leung, Y. Yam, and P. W. Y. Chiu, "18 - Applications of Flexible Robots in Endoscopic Surgery," in *Handbook of Robotic and Image-Guided Surgery*, M. H. Abedin-Nasab, Ed. Elsevier, 2020.

[10] I. Ebert-Uphoff and G. Chirikjian, "Inverse kinematics of discretely actuated hyper-redundant manipulators using workspace densities," in *Proceedings of IEEE International Conference on Robotics and Automation*, vol. 1, Apr. 1996, pp. 139–145 vol.1.

[11] L. L. Howell, "Compliant Mechanisms," in *Encyclopedia of Nanotechnology*, B. Bhushan, Ed. Springer, Dordrecht, 2016, pp. 604–611.

[12] V. Chalvet, Y. Haddab, and P. Lutz, "A Microfabricated Planar Digital Microrobot for Precise Positioning Based on Bistable Modules," *IEEE Transactions on Robotics*, vol. 29, no. 3, pp. 641–649, Jun. 2013.

[13] M. Hafez, M. Lichter, and S. Dubowsky, "Optimized binary modular reconfigurable robotic devices," *IEEE/ASME Transactions on Mechatronics*, vol. 8, no. 1, pp. 18–25, Mar. 2003.

[14] G. Chen, Q. T. Aten, S. Zirbel, B. D. Jensen, and L. L. Howell, "A Tristable Mechanism Configuration Employing Orthogonal Compliant Mechanisms," *Journal of Mechanisms and Robotics*, Feb. 2010.

[15] M. Zanaty and S. Henein, "Experimental Characterization of a T-Shaped Programmable Multistable Mechanism," *Journal of Mechanical Design*, vol. 140, no. 9, Sep. 2018.

[16] D. J. Bell, T. J. Lu, N. A. Fleck, and S. M. Spearing, "MEMS actuators and sensors: observations on their performance and selection for purpose," *Journal of Micromechanics and Microengineering*, 2005.

[17] V. D. Sars, S. Haliyo, and J. Szewczyk, "A practical approach to the design and control of active endoscopes," *Mechatronics*, 2010.

[18] Y. Goergen, R. Chadda, R. Britz, D. Scholtes, N. Koev, P. Motzki, R. Werthschützky, M. Kupnik, and S. Seelecke, "Shape Memory Alloys in Continuum and Soft Robotic Applications," in *Conference on Smart Materials, Adaptive Structures and Intelligent Systems*. American Society of Mechanical Engineers Digital Collection, 2019.

[19] R. Shoureshi and A. Shen, "Self-powered sensory nerve system for civil structures using hybrid forisome actuators," *Proceedings of SPIE - The International Society for Optical Engineering*, Mar. 2006.

[20] K. Ikuta, M. Tsukamoto, and S. Hirose, "Shape memory alloy servo actuator system with electric resistance feedback and application for active endoscope," in *Proceedings. 1988 IEEE International Conference on Robotics and Automation*, Philadelphia, PA, USA, 1988.

[21] M. Neumann and J. Burgner-Kahrs, "Considerations for follow-the-leader motion of extensible tendon-driven continuum robots," in *IEEE International Conference on Robotics and Automation (ICRA)*, 2016.

[22] P. W. Henselmans, S. Gottenbos, G. Smit, and P. Breedveld, "The MemoSlide: An explorative study into a novel mechanical follow-the-leader mechanism," *Proceedings of the Institution of Mechanical Engineers, Part H: Journal of Engineering in Medicine*, 2017.

[23] H. Hussein, P. Le Moal, R. Younes, G. Bourbon, Y. Haddab, and P. Lutz, "On the design of a preshaped curved beam bistable mechanism," *Mechanism and Machine Theory*, vol. 131, 2019.

[24] H. Hussein, P. Moal, G. Bourbon, Y. Haddab, and P. Lutz, "Modeling and Stress Analysis of a Pre-Shaped Curved Beam : Influence of High Modes of Buckling," *International Journal of Applied Mechanics*, vol. 7, no. 4, p. 20 p, 2015.

[25] S. P. Timoshenko and J. M. Gere, *Theory of Elastic Stability*. New York: McGraw-Hill, 1961.

[26] L. Rubbert, R. Bitterli, N. Ferrier, S. Fifanski, I. Vardi, and S. Henein, "Isotropic springs based on parallel flexure stages," *Precision Engineering*, vol. 43, pp. 132–145, Jan. 2016.

[27] S. Timoshenko, *History of Strength of Materials: With a Brief Account of the History of Theory of Elasticity and Theory of Structures*. Courier Corporation, Jan. 1983.

[28] M. Ben Salem, G. Aiche, Y. Haddab, L. Rubbert, and P. Renaud, "Additive Manufacturing of a Bistable Mechanism Using Fused Deposition Modeling: Experimental and Theoretical Characterization," in *MR 2019 - 43rd Mechanisms and Robotics Conference @IDETC-CIE*. United States: American Society of Mechanical Engineers, Aug. 2019.

[29] A. Damani, "An Empirical Model of Piezoelectric Stick-Slip Actuation Of The KLEINDIEK MM3A Micromanipulator," Ph.D. dissertation, University of Utah, Utah, 2013.

[30] B. Calmé, L. Rubbert, and Y. Haddab, "Towards a compact and low-cost mesoscopic XY positioning system using 3D printing of conductive polymers," in *2022 International Conference on Manipulation, Automation and Robotics at Small Scales (MARSS)*, 2022.

[31] M. Zanaty, T. Fussinger, A. Rogg, A. Lovera, D. Lambelet, I. Vardi, T. J. Wolfensberger, C. Baur, and S. Henein, "Programmable Multistable Mechanisms for Safe Surgical Puncturing," *Journal of Medical Devices*, vol. 13, no. 2, Jun. 2019.